Lipid bilayers driven to a wrong lane in molecular dynamics simulations by truncation of long-range electrostatic interactions

Michael Patra and Mikko Karttunen
Biophysics and Statistical Mechanics Group, Laboratory of Computational Engineering, Helsinki University of Technology, P.O. Box 9203, FIN–02015 HUT, Finland

Marja T. Hyvönen
Wihuri Research Institute, Kalliolinnantie 4, FIN–00140 Helsinki, Finland, and Laboratory of Physics and Helsinki Institute of Physics Helsinki University of Technology, P.O. Box 1100, FIN–02015 HUT, Finland

Emma Falck and Ilpo Vattulainen
Laboratory of Physics and Helsinki Institute of Physics, Helsinki University of Technology, P.O. Box 1100, FIN–02015 HUT, Finland

(Dated: April 8, 2003)

We provide compelling evidence that different treatments of electrostatic interactions in molecular dynamics simulations may dramatically affect dynamic properties of lipid bilayers. To this end, we consider a fully hydrated pure dipalmitoylphosphatidylcholine (DPPC) bilayer through 50 ns molecular dynamics simulations and study various dynamic properties of individual lipids in a membrane, including the velocity autocorrelation function, the lateral and rotational diffusion coefficients, and the autocorrelation function for the area per molecule. We compare the results based on the Particle-Mesh Ewald (PME) technique with those obtained by an approach where the electrostatic interactions are truncated at $r_{\rm cut} = 1.8$, 2.0, and 2.5 nm, and find that all examined truncation methods lead to results distinctly different from those obtained by PME. The lateral diffusion coefficients obtained by PME and truncation at 1.8 nm, for example, differ by a factor of 10, while the PME results are consistent with experimental values. The observed deviations can be interpreted in terms of artificial ordering due to truncation, and highlight the important role of electrostatic interactions in the dynamics of systems composed of lipids and other biologically relevant molecules such as proteins and DNA.

I. INTRODUCTION

Electrostatics plays a crucial role in numerous soft-matter systems, including the properties of water, structure of proteins and DNA and self-assembly and overcharging of DNA-lipid complexes [1, 2, 3, 4, 5, 6, 7]. Lipids in particular are an excellent example since they form stable structures such as bilayers, which serve as mattresses for proteins embedded in cell membranes [8, 9, 10, 11, 12]. Furthermore, lipids are involved in processes such as gene and drug transfer facilitated by liposomes that are essentially lipid bilayers [13, 14].

In the above examples, the properties of biological systems in question are strongly influenced by *long-range electrostatic interactions*. This is a crucial issue in computational modeling, as techniques such as classical molecular dynamics (MD) have become a common tool for studies of macromolecular systems at an atomic level [15, 16]. Thus, proper treatment of electrostatic interactions is acknowledged as one of the most important issues in MD simulations, and there has been a substantial amount of work to develop reliable and efficient methods to this end [17].

In this regard, there are techniques such as the Ewald summation (and its variants) [18]and the fast multipole method [15, 19] which are based on solving the Poisson equation for the electrostatic potential such that all charged particles and their periodic images are taken into account in a systematic fashion. In particular, the Particle-Mesh Ewald (PME) technique [15, 20] has been applied increasingly often in MD studies of soft-matter systems.

Alternatively, one can neglect the long-range Coulombic tail and truncate the interactions at some suitable distance, a typical choice being 1.4 – 2.0 nm. This approach is appealing since it leads to considerable savings in the computational cost. Consequently, it is frequently used when computational requirements are substantial due to large system sizes or long time scales, which may be the case, e.g., in studies of lipid-protein systems [21], self-assembly of lipids [22], and membrane fusion [23]. Unfortunately, this speed-up does not come for free. It has been shown that the truncation of electrostatics is associated with certain *artifacts in structural properties of biological molecules*. For example, the structural properties of water both in bulk [24, 25, 26] and close to lipid monolayers [25, 27, 28] have been found to be affected by the truncation of electrostatic interactions. Other cases where similar structural effects have been observed include peptides [29, 30], proteins [31], DNA [32, 33], and most recently lipid bilayers [34, 35].

In view of the importance of membranes for numerous cellular processes, it is very surprising that the influence of electrostatic interactions on *lipid bilayers* has been in the spotlight only very recently. Venable et al. considered a one-component dipalmitoylphosphatidylcholine (DPPC) bilayer in the low-temperature gel state using both PME and truncation at 1.2 nm, and found [34] that the results for the area per molecule differed by about 4 %. More recently, we focused on a DPPC bilayer in a physiologically more relevant liquid-crystalline phase and found that various structural properties exhibit major artifacts due to the truncation of electrostatic interactions [35]. For example, when the PME results were compared to those obtained using a truncation at 1.8 nm, the results for the area per lipid molecule differed by about 15 %,

and the results for the order parameter characterizing the orientational order of lipid acyl chains varied by about 45 %. In both cases, the PME results were in agreement with experimental data. The size of these artifacts is simply astounding, yet the underlying reason is very simple: Truncation leads to artificial ordering in the plane of the membrane [35], which implies that the phase behavior of the system is different from the desired one. If this is the case, then it is clear that essentially all structural properties of any lipid bilayer system deviate from their true behavior.

These findings give rise to the interesting question of how important is the proper treatment of electrostatic interactions for *dynamic properties* in biologically relevant soft-matter systems. Rather surprisingly, this question has not been addressed in the case of lipid bilayer systems at all, yet the dynamics of lipid bilayers have the key role in processes such as lateral diffusion, membrane fusion, and permeation. Due to the central role of membranes in regulating various cellular processes through the function of proteins, the correct description of electrostatics for membrane dynamics is particularly important. Besides this, during the last year or so dynamic properties of lipid systems have become a very topical issue since, MD simulations of the order of 50 – 100 ns are now possible [22, 23]. These time scales allow, for the first time, studies of complex dynamic processes associated with membranes, such as fusion and self-assembly, among others.

In this article, we show through an extensive set of 50 ns MD simulations for a fully hydrated pure lipid bilayer of 128 DPPC molecules in the liquid-crystalline phase that *truncation of electrostatic interactions can have dramatic consequences on the dynamic properties of lipid bilayer systems*. We consider several truncation distances from 1.8 to 2.5 nm and compare the results to those obtained using the Particle-Mesh Ewald technique. We consider several dynamic properties of individual lipid molecules, including the lateral and rotational diffusion as well as the autocorrelation function of the area per lipid. We find that the truncation method leads to distinctly different results as compared to a case where PME has been applied. The lateral diffusion serves as an excellent example of this fact, since *deviations between the truncation methods and PME were observed on all time scales studied*, and quantified eventually in the lateral diffusion coefficient which for a truncation at 1.8 nm differed from the PME result by a factor of 10. The PME result is consistent with experimental values. The deviations between truncation and PME persist even for large truncation distances. This strongly suggests that the artifacts due to truncation are systematic and cannot be cured by increasing the cutoff distance.

II. SYSTEM

A. Model and simulation details

We have considered a one-component lipid bilayer consisting of $N = 128$ DPPC molecules fully hydrated by 3655 water molecules. The initial bilayer configuration made up of DPPC molecules corresponds to the final structure of run E presented in Ref. [36] (available at `http://moose.bio.ucalgary.ca/files/dppc128.pdb`), and the principal axes of the system are chosen such that the bilayer is in the x-y plane. The united atom model description used in this work has been considered previously by Tieleman et al. [36] and validated in a more recent MD study [35].

The parameters for bonded and non-bonded interactions were taken from a rather recent study on a DPPC bilayer system [37], available in electronic form at `http://moose.bio.ucalgary.ca/files/lipid.itp`. The partial charges were obtained from the underlying model description [36] and can be found at `http://moose.bio.ucalgary.ca/files/dppc.itp`. For water, we used the SPC model [38].

An approach commonly adapted in lipid bilayer simulations is to calculate electrostatic interactions within a certain distance (usually about 1.0 nm) at each time step, while interactions beyond this range are determined every k timesteps ($k \gg 1$). There are two commonly used approaches known as the multiple time step (MTS) and the twin-range cutoff (TRC) schemes. (The notations are not fully established, and are discussed in Ref. [39].) Both schemes evaluate long-range forces only once every k steps. In MTS, the velocities are updated in steps $1, \ldots, k-1$ only from the short-range forces, and only during the step k the velocity is updated also from the long-range forces. In TRC the velocity is updated at each time step also from the long-range forces, though it is assumed to be constant within each cycle of k steps.

It can be expected that TRC should give slightly "more accurate" trajectories, while MTS offers the advantage that time-reversal symmetry is observed more appropriately than in the TRC scheme. For this reason, k is usually limited to about 10 in TRC, while MTS would allow significantly larger k.

In this work, we have used a scheme where electrostatic interactions within 1.0 nm were calculated at each time step, while interactions beyond this range were determined every $k = 10$ timesteps by TRC. This choice is supported by a number of reasons. First, due to the relatively small k applied by us, the problem of how to best divide the forces into long-range and short-range components is not as important as in the MTS schemes. Second, these choices follow the parameterization of DPPC by Tieleman and Berendsen [36]. In addition, since basically all DPPC simulations reported so far have used a twin-range scheme and our objective is to use an approach that is common in this field, we decided to follow the same idea.

For the range of electrostatics we have chosen two possible ways: Group-based long-range electrostatic interactions were handled either by using a cutoff at $r_{\mathrm{cut}} = 1.8$ nm, 2.0 nm, or 2.5 nm, or by means of the Particle-Mesh Ewald [15, 20] method to take the long-range interaction fully into account. Finally, Lennard-Jones interactions were cut off at 1.0 nm without switch functions.

The simulations were performed using the Gromacs [40] package in the NpT ensemble using a time step of 2.0 fs. The Berendsen algorithm with a time constant of 1 ps for pressure coupling was used as barostat. The setup was chosen such that the height of the simulation box (i. e., its extension in the

z-direction) was allowed to vary independently of the cross-sectional area of the box in the x-y plane. The DPPC and water molecules were separately coupled to a heat bath at temperature $T = 323\,\mathrm{K}$ using the Berendsen algorithm [41] with a coupling constant of 0.1 ps. The lengths of all bonds were kept constant with the Lincs algorithm [42].

Typical time scales studied in recent MD simulations of lipid bilayer systems have been of the order of $3-20\,\mathrm{ns}$ [43, 44, 45, 46, 47]. These time scales can provide one with a great deal of insight into the structural properties of membrane systems. In the case of dynamics, however, the computational requirements are appreciably more demanding. In the present work, the simulations in each case have been extended over a time scale of 50 ns. While this time scale is large compared to the current trend, it is still relatively short compared to time scales associated with complex dynamic processes such as self-assembly and long-range undulations of lipid bilayers, which take place over time scales of the order of 100 ns [22, 48, 49]. Despite this shortcoming, we show below that the present multi-nanosecond study allows us to analyze various dynamic processes in full detail, and to quantify artifacts in dynamic quantities due to the truncation of electrostatic interactions.

The simulations reported in this work took about 20 000 CPU hours in total. This includes simulations at different temperatures, with various coupling constants for the barostat and the thermostat, and with different truncation distances for van der Waals interactions to confirm the validity of our results [35].

III. RESULTS AND DISCUSSION

A. Area per molecule and radial distribution functions

Before a thorough discussion of dynamics, let us first consider two important quantities that will shed some light on the origin of the artifacts. The first of them, the area per molecule, is a central quantity in membrane systems. Besides the fact that it is one of the few quantities that can be determined accurately from experiments, area fluctuations in a bilayer are related to the compressibility of the bilayer, which plays an important role in processes such as lateral diffusion, hole formation, and permeation. The second quantity, radial distribution function, in turn, is an important quantity in all soft-matter systems. Assuming that the structure of lipid bilayers is influenced by the way the electrostatics is treated in MD simulations, it is clear that the radial distribution function should show corresponding artifacts.

Results in Fig. 1 illustrate the time dependence of the area per DPPC molecule $A(t)$ over a time scale of 50 ns. We find that the equilibration of $A(t)$ takes about 10 ns, and thus we have discarded this part of the trajectory and used only the last 40 ns for analysis. The simulations using PME yield $\langle A \rangle = (0.655 \pm 0.010)\,\mathrm{nm}^2$. This is consistent with recent experiments [11], which for DPPC give $\langle A \rangle = 0.64\,\mathrm{nm}^2$. Truncation at 2.5 nm leads to $\langle A \rangle = (0.604 \pm 0.009)\,\mathrm{nm}^2$, which deviates about 8 % from the PME result. Decreasing the cutoff

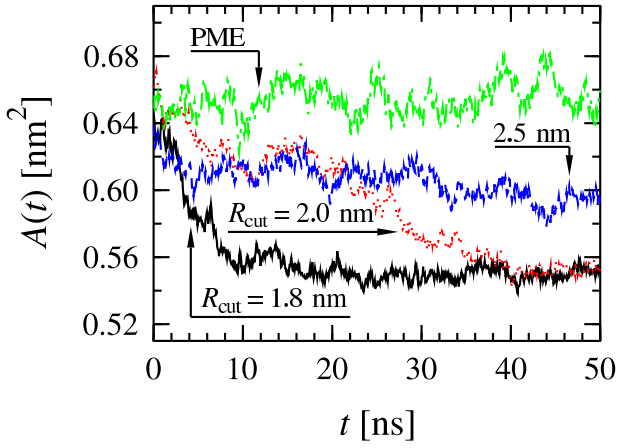

FIG. 1: Evolution of the area per molecule in time.

distance to 2.0 nm leads to $\langle A \rangle = (0.582 \pm 0.027)\,\mathrm{nm}^2$, which should be taken with some caution as the area per molecule in this case seems to have a systematic drift to smaller values. However, we found that $A(t)$ increases at times beyond 40 ns, indicating that the decrease of $A(t)$ between 20 and 40 ns is likely due to statistical fluctuations (see discussion in Sect. III B). Finally, simulations using truncation at $r_{\mathrm{cut}} = 1.8\,\mathrm{nm}$ yielded $\langle A \rangle = (0.551 \pm 0.005)\,\mathrm{nm}^2$.

The artifacts in the area per molecule, and in other structural quantities, are discussed in more detail in Ref. [35]. Instead of discussing them any further in this work, we rather note that the artifacts are essentially due to truncation of electrostatics, which leads to artificial ordering in the plane of the membrane. This is demonstrated in Fig. 2 by the intermolecular radial distribution function (RDF) $g(r)$ for the N–P pair between nitrogen and phosphate atoms in the headgroups. While PME yields an RDF which has essentially no structure beyond $r = 1.0\,\mathrm{nm}$, the RDFs of truncation schemes have a pronounced dip exactly at the truncation distance. As was shown in Ref. [35], similar conclusions on artificial ordering can be drawn for N–N and P–P pairs, in which cases the artifacts in the RDFs are even stronger. What is even more alarming is the fact that similar artificial peaks at r_{cut} were observed for the RDF of the CM positions of the lipids [35].

We conclude that the artifacts in structural quantities are due to the fact that truncation of electrostatic interactions gives rise to artificial ordering in the bilayer plane, thus changing the phase behavior of the system. In the remaining part of this work, we investigate the influence of truncation on the *dynamics of a lipid bilayer*. As we will find, the truncation leads to dramatic artifacts in various dynamic quantities.

B. Decay of the area autocorrelation function

As the first dynamic quantity, we consider the area fluctuations by following the autocorrelation function

$$C_A(t) \equiv \frac{1}{N} \sum_{i=1}^{N} \frac{\langle A_i(t+t') A_i(t') \rangle - \langle A_i \rangle^2}{\langle A_i^2 \rangle - \langle A_i \rangle^2}, \qquad (1)$$

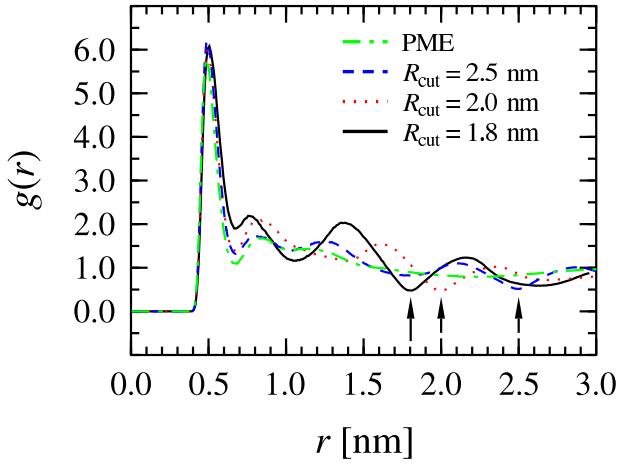

FIG. 2: Radial distribution function for intermolecular P – N pairs in the head groups of the DPPC molecules. Note the dips exactly at the truncation distance as shown by the arrows.

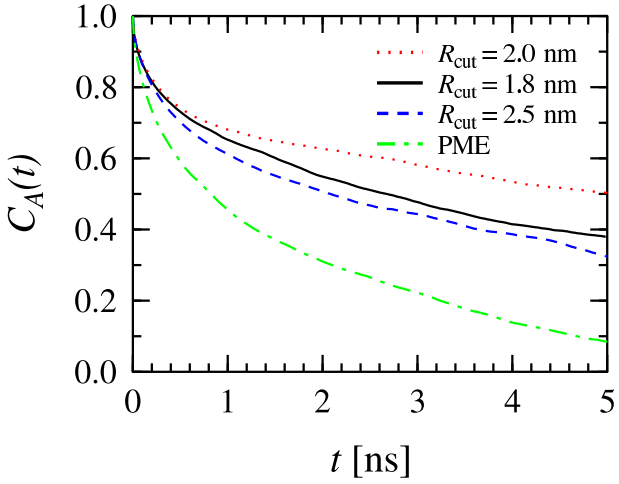

FIG. 3: Results for the decay of the area autocorrelation function based on the Voronoi analysis in 2D.

Time	1.8 nm	2.0 nm	2.5 nm	PME
τ	7.1 ± 0.6	12.3 ± 2.4	7.4 ± 2.7	2.5 ± 1.8
$t_{1/2}$	2.7 ± 0.6	5.0 ± 0.6	2.1 ± 1.1	0.70 ± 0.07

TABLE I: Characteristic times τ and $t_{1/2}$ (in units of nanoseconds) describing the decay of the area autocorrelation function $C_A(t)$.

where $A_i(t)$ is the area of the molecule i ($i = 1, \ldots, N$) at time t, and $\langle\ \rangle$ denotes a time-average over a large number of configurations.

To calculate the area occupied by each individual lipid, $A_i(t)$, we applied the Voronoi analysis in two dimensions [50]. We first computed the center of mass (CM) positions for the lipids and projected them onto the x-y plane. A point in the plane is then considered to belong to a particular Voronoi cell if it is closer to the projected CM of the lipid molecule associated with that cell than to any other CM position.

Results in Fig. 3 show that the area autocorrelation function decays on a time scale of few nanoseconds. After a narrow initial regime of about 0.5 – 1 ns, the decay of $C_A(t)$ follows an exponential via $C_A(t) \sim \exp(-t/\tau)$. For the characteristic decay time (τ), results shown in Table I indicate that the area autocorrelation function based on the truncation schemes decays much more slowly than that computed using PME. In addition, while the results of 1.8 nm and 2.5 nm are essentially identical, the case of 2.0 nm differs somewhat from the general trend. We expect that this is due to the drift of $A(t)$ in Fig. 1 illustrating the common view that simulations using truncation are less stable compared to those using PME and its variants. This, too, should give rise to concern as it casts doubt for the commonly made estimates ($\sim 1 - 5$ ns) of equilibration times in MD simulations of lipid bilayers. The autocorrelation times for area fluctuations shown in Table I support this idea.

Depending on the truncation distance, the characteristic decay time differs by a factor of 3 – 5 from the PME result. The half-times $t_{1/2}$ defined through $C_A(t_{1/2}) = 1/2$ show the same trend (see Table I). For comparison, we note that the PME result for $t_{1/2}$ is in agreement with the results of Shinoda and Okazaki [50], who used Ewald summation for a DPPC bilayer.

The present results for the decay of area fluctuations allow us to conclude that the truncation method does influence the collective dynamics of lipid bilayers. In particular, as the correlation time of area fluctuations is significantly influenced by truncation, it is clear that it has implications for processes such as permeation through lipid bilayers.

C. Lateral diffusion of lipid molecules

Lateral diffusion plays an important role in various physiologically important processes such as ordering of multicomponent lipid bilayers, endocytosis, and signaling within a lipid bilayer [51, 52]. It is also one of the mechanisms which control diffusion through membranes, e.g., the formation of ion channels is governed in part by the lateral diffusion of proteins embedded in a bilayer. As these examples illustrate, it is clear that lateral diffusion is one of the key processes which characterize the dynamics of individual molecules in a cell membrane.

To quantify the motion of single molecules in the plane of a membrane, let the CM position of lipid i at time t be $\vec{r}_i(t)$. The lateral diffusion coefficient is then defined through the Einstein relation [53]

$$D_T = \lim_{t\to\infty} \frac{1}{2dt} \langle [\vec{r}(t)]^2 \rangle, \tag{2}$$

where $d = 2$ is the dimensionality of the bilayer and $\langle [\vec{r}(t)]^2 \rangle$ is the mean-squared displacement

$$\langle [\vec{r}(t)]^2 \rangle \equiv \frac{1}{N} \sum_{i=1}^{N} \langle [\vec{r}_i(t) - \vec{r}_i(0)]^2 \rangle \tag{3}$$

averaged over all the N molecules in a bilayer.

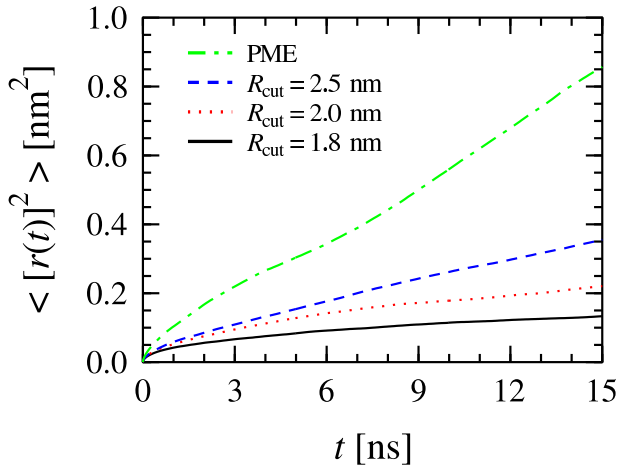

FIG. 4: Results for the mean-square displacement in time.

It is worthwhile pointing out that the center of mass positions of the two monolayers may fluctuate in time. If this drift is not accounted for, the results may reflect the motion of the monolayer's CM rather than the diffusion of individual molecules. We have paid particular attention to account for this matter by calculating the lateral diffusion coefficient in the absence of any flow, i.e., we follow the position of lipid i in the upper (lower) monolayer with respect to the center of mass position of the corresponding upper (lower) monolayer.

Results shown in Fig. 4 for the mean-square displacement show that there are major differences between the different treatments of long-range electrostatic interactions. Deviations between the different cases appear already at short times, and become increasingly apparent at longer times. When the long-time behavior is analyzed in detail in order to determine the lateral diffusion coefficient, we obtain the results shown in Table II. It is evident that the lateral diffusion coefficient based on PME is substantially larger compared to cases based on the truncation of electrostatics. In particular, PME yields a lateral diffusion coefficient which is about *ten times larger* than the result found by truncation at 1.8 nm. For larger cutoff distances we find that the lateral diffusion coefficients increase, though a systematic difference between truncation and PME results persists. Even for the largest truncation distance of 2.5 nm, which is about 40 % of the linear system size in this case, the diffusion results deviate from PME by a factor of about 2.6.

The importance of the differences between PME and truncation methods can be illustrated by a brief comparison to experimental findings. Almeida et al. used the fluorescence recovery after photobleaching (FRAP) technique to measure lateral diffusion in a pure DMPC bilayer above the main transition temperature. They found that the lateral diffusion coefficient increased by a factor of 3.5 *if the temperature was increased by 32 degrees* from 299 K to 331 K [54]. For a DLPC-cholesterol bilayer mixture Korlach et al. found [55] the lateral diffusion rate to decrease by a factor of 10 *if the cholesterol concentration was increased from 0 % to 60 %*. In these systems the changes in lateral diffusion were caused by major changes in their thermodynamic state. As the truncation of electrostatic interactions—and not a change in physical conditions—can lead to changes having the same magnitude, it is obvious that one should exercise great care when using truncation methods.

Electrostatics	D_T [cm^2 / s]
Truncation at 1.8 nm	$(1.3 \pm 0.3) \times 10^{-8}$
Truncation at 2.0 nm	$(3.0 \pm 0.3) \times 10^{-8}$
Truncation at 2.5 nm	$(4.9 \pm 0.4) \times 10^{-8}$
PME	$(12.7 \pm 0.5) \times 10^{-8}$
FRAP [56]	12.5×10^{-8}
QENS [57, 58]	10×10^{-8}
FRAP [54]	13×10^{-8}

TABLE II: Lateral diffusion coefficients D_T describing the motion of DPPC molecules in the plane of the bilayer. Experimental values are also given for the purpose of comparison: FRAP experiments [56] for a DPPC bilayer at $T = 323$ K, QENS measurements [57, 58] for a DPPC system at $T = 333$ K, and FRAP experiments [54] at $T = 323$ K for a DMPC system.

We would like to stress that different experimental techniques usually probe diffusion over a wide range of different time scales. As far as long-range diffusion over long time scales is concerned, the most appropriate comparison in the present case can be made to FRAP and "long-range" quasi-elastic neutron scattering (QENS) measurements. Our findings using the PME scheme are consistent with these experimental values (see Table II).

The present results demonstrate very clearly the subtle nature of electrostatic interactions. We have found that even seemingly minor changes in the treatment of electrostatic interactions can have dramatic consequences in transport coefficients defined over long times and large distances. The results based on truncation are distinctly different from those obtained by PME. Even large cutoff distances comparable to the half of the linear size of the system lead to results systematically different from PME results.

D. Velocity autocorrelation function

Alternatively, lateral diffusion of individual molecules can be described by the velocity autocorrelation function

$$\phi(t) \equiv \frac{1}{N} \sum_{i=1}^{N} \langle \vec{v}_i(t+t') \cdot \vec{v}_i(t') \rangle, \tag{4}$$

where $\vec{v}_i(t)$ is the CM velocity of molecule i at time t. In principle, the lateral diffusion coefficient can then be defined through the Green-Kubo equation [53]

$$D_T = \frac{1}{d} \int_0^\infty \mathrm{d}t \, \phi(t). \tag{5}$$

In practice, however, this approach to calculate D_T is rather difficult due to the fact that the characteristic decay time of

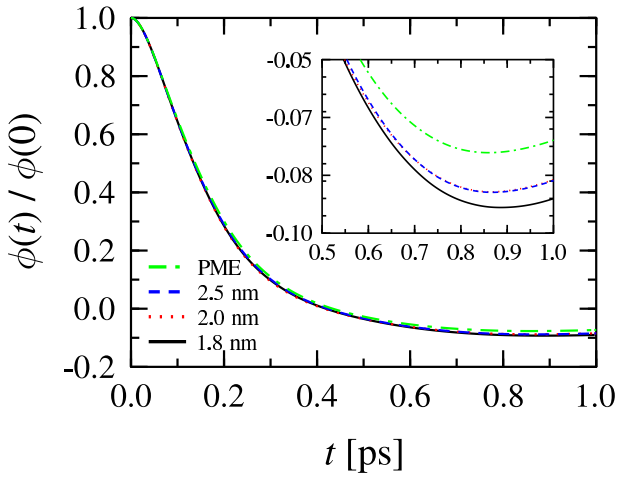

FIG. 5: The normalized velocity autocorrelation function $\phi(t)/\phi(0)$ vs. time. The deviations between the different schemes are illustrated in more detail in the inset. Note that the curve of 2.0 nm in the inset is essentially on top of the curve of 2.5 nm.

Electrostatics	Case (a): $D_{\rm eff}$ [cm^2/s]
Truncation at 1.8 nm	$(1.226 \pm 0.022) \times 10^{-5}$
Truncation at 2.0 nm	$(1.227 \pm 0.037) \times 10^{-5}$
Truncation at 2.5 nm	$(1.252 \pm 0.015) \times 10^{-5}$
PME	$(1.352 \pm 0.012) \times 10^{-5}$
Electrostatics	**Case (b): $D_{\rm eff}$ [cm^2/s]**
Truncation at 1.8 nm	$(1.11 \pm 0.04) \times 10^{-6}$
Truncation at 2.0 nm	$(1.19 \pm 0.04) \times 10^{-6}$
Truncation at 2.5 nm	$(1.23 \pm 0.03) \times 10^{-6}$
PME	$(1.57 \pm 0.02) \times 10^{-6}$

TABLE III: Effective lateral diffusion coefficients $D_{\rm eff}$ found by integrating the velocity autocorrelation function from (a) zero to 1 ps and from (b) zero to 10 ps [see Eq. (5) and Fig. 5].

$\phi(t)$ is usually very small, whereas the convergence of the integral in Eq. (5) takes a long time. In the present case for a DPPC bilayer, we found that the characteristic decay time of $\phi(t)$ is about 0.2 ps, while the convergence was achieved on a time scale of the order of 2 – 5 ns. This implies that an accurate determination of D_T through Eq. (5) requires $\phi(t)$ to be sampled at very short time intervals up to large times, which is not meaningful.

We have used the velocity autocorrelation function to quantify the size of artifacts in dynamic quantities at *short times*. The diffusion behavior in this regime corresponds to motion known as "rattling in a cage", where the molecule in question goes through conformational changes, while its CM position does not fluctuate much compared to the size of the molecule in the bilayer plane. The short-time behavior thus complements the above results for the lateral diffusion coefficient describing dynamics over long times.

In Fig. 5 we show the velocity autocorrelation function at short times up to 1 ps. We find that the difference between PME and the different truncation schemes is minor but systematic. The decay of $\phi(t)$ is fastest in the case of $r_{\rm cut} = 1.8$ nm, followed by truncation distances of 2.0 and 2.5 nm, while PME leads to the slowest decay. As D_T is an integral of $\phi(t)$, these results are consistent with our findings in Sect. III C.

If we integrate $\phi(t)$ up to 1 ps (instead of very large times), we find effective diffusion coefficients $D_{\rm eff}$ on the scale of 1×10^{-5} cm^2/s (see Table III). The deviations between the truncation schemes compared to PME are surprisingly large (7 – 10 %) given that the time scale is very short and does not allow large displacements in the plane of the membrane. Nevertheless, the results imply that diffusion at very short time scales is not strongly influenced by the truncation of electrostatic interactions, since the deviations in Table III are significantly smaller compared to those for lateral diffusion reported in Table II for D_T.

If $\phi(t)$ is considered up to 10 ps, one finds (see Table III) the effective diffusion coefficients to be on a scale of 1×10^{-6} cm^2/s, the deviations between PME and the truncation schemes being about 21 – 29 %. In this case a direct comparison to experimental data is difficult, though the value 4×10^{-6} cm^2/s obtained by short-time ("local") QENS measurements [59] for DPPC at 336 K indicates that our results are on the same scale.

It is clear that the differences in the lateral diffusion coefficient D_T come mainly from the long-time behavior of $\phi(t)$, as the diffusion of lipid molecules becomes increasingly influenced by the artifacts due to electrostatics. The question is, do the deviations between the different schemes increase uniformly in time, or is there some characteristic time scale related to molecular diffusion mechanisms above which the artifacts in $\phi(t)$ become very pronounced over a short time scale?

E. Distribution of lateral displacements

To clarify this issue, let us consider the distribution of particle displacement lengths over some fixed time scale. We denote the CM position of particle i at time t by $\vec{r}_i(t)$ and let it diffuse over a time period δt to position $\vec{r}_i(t+\delta t)$. Since the bilayer is in the x-y plane, the projection of the particle position onto the bilayer plane, $\vec{r}_{i,\rm 2D}(t)$, defines the particle displacement $\delta\vec{r}_{i,\rm 2D}(\delta t) = \vec{r}_{i,\rm 2D}(t+\delta t) - \vec{r}_{i,\rm 2D}(t)$ whose length is denoted by $\ell_i(\delta t)$. As in Sect. III C, the drift of the monolayer's CM has been accounted for in the analysis. The displacements $\ell_i(\delta t)$ make up a particle displacement distribution function $P_i(\ell, \delta t)$. When averaged over all the N molecules, one obtains $P(\ell, \delta t) = (1/N) \sum_{i=1}^{N} P_i(\ell, \delta t)$.

The second moment of $P(\ell, \delta t)$ at long times yields the lateral diffusion coefficient D_T. Here we use $P(\ell, \delta t)$ to quantify deviations between different cases by the average particle displacement

$$\ell_{\rm ave}(\delta t) \equiv \int_0^\infty {\rm d}\ell \, P(\ell, \delta t) \ell, \qquad (6)$$

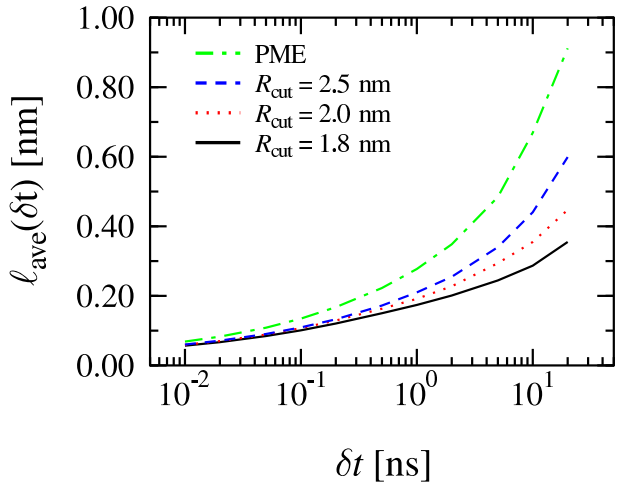

FIG. 6: Average particle displacements $\ell_{\rm ave}(\delta t)$ over a fixed time period δt.

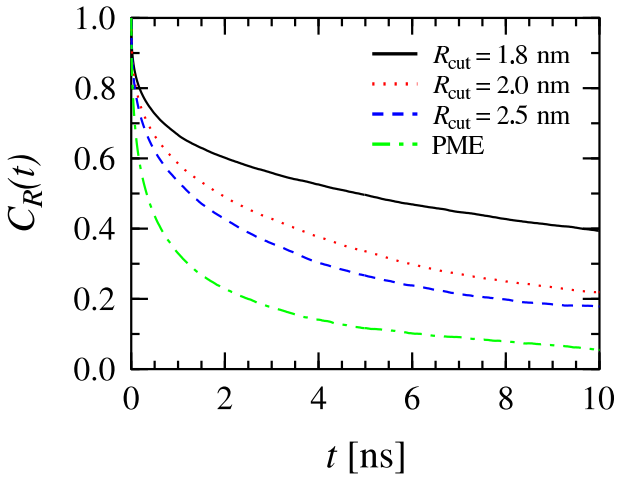

FIG. 7: The correlation function of rotational diffusion $C_R(t)$ for the unit vector $\vec{\mu}(t)$ along the P – N vector in the headgroup of DPPC. At long times one expects $C_R(t) \sim \exp(-t/\tau_R)$.

which describes how far, on average, a given particle moves during time δt. This is a suitable measure especially at short times: While quantities like $\sqrt{2\,d\,D_T \delta t}$ are often used for this purpose, they are valid only at large times in the diffusive regime, i.e., where $\langle[\vec{r}(t)]^2\rangle \sim t$.

The results for the average displacement $\ell_{\rm ave}(\delta t)$ are summarized in Fig. 6. For times up to $\delta t = 50$ ps, the average displacement obtained by the truncation schemes deviates by 15 – 30 % from the PME result. At the same time, the results based on different truncation distances are approximately similar up to $\delta t = 100$ ps. Most remarkably, however, we find that the deviations between the different schemes increase uniformly in time.

Further studies of $P(\ell, \delta t)$ (data available in Supporting Information) indicate that it is strongly affected by the treatment of electrostatics. Already at short times of the order of 10 ps, the distribution functions of truncation schemes are distinctly different from PME, the main difference being in the long-distance tail.

Based on these findings for lateral diffusion, velocity correlations, and lateral displacements in Sects. III C – III E we may conclude that the dynamics of lipid molecules in the plane of the membrane depend clearly on the treatment of electrostatic interactions. The truncation schemes, in general, lead to results biased from those obtained by PME. These differences are apparent not only at large times, but they are pronounced even at short times (of the order of 1 – 10 ps) where $\ell_{\rm ave}$ is less than 10% of the size of the molecule. This allows us to conclude that *electrostatics plays a role at all time scales*, including even the very short ones where lateral diffusion corresponds to motion known as "rattling in a cage".

F. Rotational diffusion

Besides lateral diffusion, the motion of lipid molecules can be described by their rotational degrees of freedom and characterized by the so-called rotational diffusion coefficient D_R. To this end, one often considers Wigner rotation matrices [60] such as the $C_2(t)$ correlation function

$$C_2(t) \equiv \frac{1}{2}\langle 3[\vec{\mu}(t)\cdot\vec{\mu}(0)]^2 - 1\rangle, \qquad (7)$$

where $\vec{\mu}(t)$ is the unit vector of some chosen rotational mode at time t. At long times, one expects the decay $C_2(t) \sim \exp(-t/\tau_R)$ to yield the rotational diffusion coefficient via $\tau_R \propto 1/D_R$. This approach is particularly common in experiments such as the nuclear magnetic resonance technique.

In the present work, we have focused on three vectors that describe different aspects of rotational motion. First, we consider the P – N vector in the phosphocholine head group. Second, we examine the rotational diffusion of the glycerol group, characterized by a unit vector from the *sn*–1 carbon to the *sn*–3 carbon in a DPPC molecule (see Fig. 1 in Ref. [35]). Finally, we characterize the rotational diffusion of acyl chains, in which case the unit vector is drawn from the first to the last carbon in the *sn*–1 chain.

Results in Fig. 7 demonstrate the decay of $C_2(t)$ for the P – N vector. At early times, the results based on PME decay very rapidly, the half-time $t_{1/2}$ (defined as $C_2(t_{1/2}) = 1/2$) being about 0.33 ns. The results based on truncation methods, on the other hand, decay much more slowly as is demonstrated by the value of $t_{1/2} = 4.9$ ns with $r_{\rm cut} = 1.8$ nm. At longer times from 5 to 10 ns we find $1/\tau_R = 0.143\,{\rm ns}^{-1}$ for PME, and $0.045\,{\rm ns}^{-1}$ for 1.8 nm.

Results for the characteristic times are summarized in Table IV. Largest deviations between PME and the truncation methods are found in the rotational time scales of the *sn*–1 tail. Then, both the early and the long time behavior deviate by a factor which ranges around *one order of magnitude*.

The time scale of 50 ns studied in this work is not long enough to find the true asymptotic regime of $C_2(t)$. Much longer time scales would be needed to find the exponential regime for $C_2(t)$ with full certainty. Thus, the values in Table IV should be regarded as suggestive. However, they do al-

P – N vector				
Time	1.8 nm	2.0 nm	2.5 nm	PME
τ_R	22.2 ± 5.4	11.9 ± 2.2	12.1 ± 2.2	7.0 ± 0.5
$t_{1/2}$	4.86 ± 0.70	1.88 ± 0.28	1.25 ± 0.12	0.33 ± 0.01
sn–1 chain				
Time	1.8 nm	2.0 nm	2.5 nm	PME
τ_R	243.0 ± 80.3	96.4 ± 18.9	89.4 ± 8.1	42.9 ± 6.6
$t_{1/2}$	> 100	7.66 ± 3.10	2.32 ± 0.36	0.75 ± 0.01
Vector from *sn*–1 to *sn*–3				
Time	1.8 nm	2.0 nm	2.5 nm	PME
τ_R	24.9 ± 5.9	16.5 ± 2.8	14.1 ± 2.0	10.2 ± 1.0
$t_{1/2}$	3.77 ± 1.08	2.14 ± 0.70	1.49 ± 0.30	0.75 ± 0.04

TABLE IV: Characteristic times τ_R and $t_{1/2}$ (in units of nanoseconds) describing the decay of the rotational autocorrelation function $C_R(t)$. Shown here are the times for the three vectors considered: The P – N vector, the vector from the first to the last carbon in the *sn*–1 chain, and the vector from the *sn*–1 carbon to the *sn*–3 carbon in the glycerol group. The times τ_R have been determined from the range between 5 and 10 ns.

low us to compare the different schemes for the electrostatics, and the message is clear: *The dynamics of rotational motion in lipid bilayers is considerably slowed down by the truncation of electrostatic interactions*.

G. Efficiency

As a final issue, let us briefly comment on the efficiency of truncation schemes compared to PME. In the present model system without parallelization, we have found that a truncation of electrostatic interactions at 1.8 nm and 2.0 nm is faster than PME by a factor of 1.8 and 1.4, respectively. Truncation at 2.5 nm, however, is slightly slower than PME. This demonstrates that large truncation distances are not desirable in systems of present size, where the efficiency of PME is actually rather reasonable.

In general the situation is more complicated. The CPU time needed for truncation schemes scales as $\mathcal{O}(N)$, or $\mathcal{O}(r_{\rm cut}^3)$, while for PME it is $\mathcal{O}(N \log N)$. Besides this, PME cannot be parallelized as efficiently as truncation methods. This implies that the truncation always becomes more efficient than PME as the size of the system or the number of parallel nodes is increased. Thus, it is likely that the use of truncation schemes will be inevitable in studies of large and complex systems, which are not doable by incorporating full electrostatics into the system in question.

IV. SUMMARY AND CONCLUSIONS

Together with current computational resources, the classical molecular dynamics (MD) technique has very recently evolved to a stage where it can be applied to various dynamic processes in complex soft-matter systems. Fusion of liposomes with flat lipid bilayers and undulations of membranes are just two of the many examples in this regard. However, due to the large systems and long time scales involved in these processes, the computational effort of studying the dynamics is substantial. To reduce the computational cost, it has become common to truncate the long-range electrostatic interactions. This has been done in spite of the evidence that the truncation may affect structural properties of soft-matter systems.

In this work, we have investigated the dynamics of DPPC lipid bilayers through multi-nanosecond MD simulations and compared the Particle-Mesh Ewald (PME) results with those of three different truncation schemes. The PME approach is clearly more costly compared to the truncation schemes—for example in the present model system the computational cost of PME has been found to be larger by a factor of 1.8 compared to a truncation at 1.8 nm. At the same time, however, we have found compelling evidence that the truncation of electrostatic interactions has a major disadvantage. The lateral diffusion rates studied by a truncation at 1.8 nm were found to deviate by one order of magnitude from the PME results. Similar deviations were found over all time scales studied, down to very short times where the lateral diffusion corresponds to short-scale motion known as “rattling in a cage”. These artifacts certainly play a role in processes where lateral re-organization of molecules in a bilayer is important. The decay rate of area per lipid fluctuations is changed almost as extensively, an artifact which certainly affects the permeation rates of small molecules through membranes. As the other dynamic quantities considered in this work support these findings, we may conclude that the truncation is not the method of choice for incorporating electrostatic interactions into model systems of lipid membranes.

While this work has focused on the dynamics of lipid bilayers, it is expected that the same conclusions apply to many other biologically relevant soft-matter systems where electrostatics plays a crucial role, such as DNA-lipid complexes and proteins in membranes. In all these cases, one should be aware of possible artifacts in both the structure and the dynamics of the molecules studied, if the truncation of electrostatic interactions is applied.

Acknowledgments. This work has, in part, been supported by the Academy of Finland through its Center of Excellence Program (E.F. and I.V.), the National Graduate School in Materials Physics (E.F.), the Academy of Finland Grants No. 54113 (M.K.), No. 80851 (M.T.H.), and No. 80246 (I.V.), the Jenny and Antti Wihuri Foundation (M.T.H.), the Federation of Finnish Insurance Companies (M.T.H.), and by the European Union through the Marie Curie fellowship HPMF–CT–2002–01794 (M.P.). We would also like to thank the Horse-Shoe (DCSC) supercluster computing facility at the University of Southern Denmark for computer resources.

[1] Ladanyi, B. M.; Skaf, M. S. *Annu. Rev. Phys. Chem.* **1993**, 44, 335–368.

[2] Koltover, I.; Salditt, T.; Rädler, J. O.; Safinya, C. R. *Science* **1998**, 281, 78–81.

[3] Bandyopadhyay, S.; Tarek, M.; Klein, M. L. *J. Phys. Chem. B* **1999**, 103, 10075–10080.

[4] Giudice, E.; Lavery, R. *Acc. Chem. Res.* **2002**, 35, 350–357.

[5] Makarov, V.; Pettitt, B. M. *Acc. Chem. Res.* **2002**, 35, 376–384.

[6] Grosberg, A. Y.; Nguyen, T. T.; Shklovskii, B. I. *Rev. Mod. Phys.* **2002**, 74, 329–345.

[7] Patra, M.; Patriarca, M.; Karttunen, M. *Phys. Rev. E* **2003**, 67, 031402.

[8] Bloom, M.; Evans, E.; Mouritsen, O. G. *Q. Rev. Biophys.* **1991**, 24, 293–397.

[9] *Structure and dynamics of membranes: From cells to vesicles*; Lipowsky, R., Sackmann, E., Eds.; Elsevier: Amsterdam, 1995.

[10] *Biological membranes: A molecular perspective from computation and experiment*; Merz, Jr. K. M., Roux, B., Eds.; Birkhäuser: Boston, 1996.

[11] Nagle, J. F.; Tristram-Nagle, S. *Biochim. Biophys. Acta.* **2000**, 1469, 159–195.

[12] *Lipid bilayers: Structure and interactions*; Katsaras, J., Gutberlet, T., Eds.; Springer-Verlag: Berlin, 2001.

[13] Langer, R. *Nature (Supp.)* **1998**, 392, 5–10.

[14] Needham, D. *MRS Bulletin* **1999**, 24, 32–40.

[15] Frenkel, D.; Smit, B. *Understanding molecular simulation: From algorithms to applications, 2nd edition.* Academic Press: San Diego, 2002.

[16] Saiz, L.; Bandyopadhyay, S.; Klein, M. L. *Bioscience Rep.* **2002**, 22, 151–173.

[17] Tobias, D. J. *Curr. Opin. Struct. Biol.* **2001**, 11, 253–261.

[18] Sagui, C.; Darden, T. A. *Annu. Rev. Biophys. Biomol. Struct.* **1999**, 28, 155–179.

[19] Greengard, L.; Rokhlin, V. *J. Comput. Phys.* **1987**, 73, 325–348.

[20] Essman, U.; Perera, L.; Berkowitz, M. L.; Darden, H. L. T.; Pedersen, L. G. *J. Chem. Phys.* **1995**, 103, 8577–8592.

[21] Zangi, R.; de Vocht, M. L.; Robillard, G. T.; Mark, A. E. *Biophys. J.* **2002**, 83, 112–124.

[22] Marrink, S. J.; Lindahl, E.; Edholm, O.; Mark, A. E. *J. Am. Chem. Soc.* **2001**, 123, 8638–8639.

[23] Marrink, S. J.; Tieleman, D. P. *Biophys. J.* **2002**, 83, 2386–2392.

[24] Alper, H. E.; Levy, R. M. *J. Chem. Phys* **91**, 1242–1251.

[25] Feller, S. E.; Pastor, R. W.; Rojnuckarin, A.; Bogusz, A.; Brooks, B. R. *J. Phys. Chem.***100**, 17011–17020.

[26] Mark, P.; Nilsson, L. *J. Comput. Chem.* **2002**, 23, 1211–1219.

[27] Alper, H. E.; Bassolino, D.; Stouch, T. R. *J. Chem. Phys.* **98**, 9798–9807.

[28] Alper, H. E.; Bassolino-Klimas, D.; Stouch, T. R. *J. Chem. Phys.* **99**, 5547–5559.

[29] Smith, P. E.; Pettitt, B. M. *J. Chem. Phys.* **1991**, 95, 8430–8441.

[30] Schreiber, H.; Steinhauser, O. *Biochemistry* **1992**, 31, 5856–5860.

[31] York, D. M.; Darden, T. A.; Pedersen, L. G. *J. Chem. Phys.* **99**, 8345–8348.

[32] York, D. M.; Yang, W.; Lee, H.; Darden, T.; Pedersen, L. G. *J. Am. Chem. Soc.* **1995**, 117, 5001–5002.

[33] Norberg, J.; Nilsson, L. *Biophys. J.* **2000**, 79, 1537–1553.

[34] Venable, R. M.; Brooks, B. R.; Pastor, R. W. *J. Chem. Phys.* **2000**, 112, 4822–4832.

[35] Patra, M.; Karttunen, M.; Hyvönen, M.; Falck, E.; Lindqvist, P.; Vattulainen, I. *Biophys. J.* **2003**, In Press; Preprint cond-mat/0211650.

[36] Tieleman, D. P.; Berendsen, H. J. C. *J. Chem. Phys.* **1996**, 105, 4871–4880.

[37] Berger, O.; Edholm, O.; Jahnig, F. *Biophys. J.* **1997**, 72, 2002–2013.

[38] Berendsen, H. J. C.; Postma, J. P. M.; van Gunsteren, W. F.; Hermans, J. In *Intermolecular Forces*; Pullman, B., Ed.; Reidel: Dordrecht, 1981; pp 331–342.

[39] Bishop, T. C.; Skeel, R. D.; Schulten, K. *J. Comput. Chem.* **1997**, 18, 1785–1791.

[40] Lindahl, E.; Hess, B.; van der Spoel, D. 2001. *J. Mol. Model.* **2001**, 7, 306–317.

[41] Berendsen, H. J. C.; Postma, J. P. M.; van Gunsteren, W. F.; DiNola, A.; Haak, J. R. *J. Chem. Phys.* **1984**, 81, 3684–3690.

[42] Hess, B.; Bekker, H.; Berendsen, H. J. C.; Fraaije, J. G. E. M. *J. Comput. Chem.* **1997**, 18, 1463–1472.

[43] Mashl, R. J.; Scott, H. L.; Subramaniam, S.; Jakobsson, E. *Biophys. J.* **2001**, 81, 3005–3015.

[44] Smondyrev, A. M.; Berkowitz, M. L. *Biophys. J.* **2001**, 80, 1649–1658.

[45] Moore, P. B.; Lopez, C. F.; Klein, M. L. *Biophys. J.* **2001**, 81, 2484–2494.

[46] Feller, S. E.; Gawrisch, K.; MacKerell, A. D. Jr. *J. Am. Chem. Soc.* **2001**, 124, 318–326.

[47] Tieleman, D. P.; Hess, B.; Sansom, M. S. P. *Biophys. J.* **2002**, 83, 2393–2407.

[48] Lindahl, E.; Edholm, O. *Biophys. J.* **2000**, 79, 426–433.

[49] Marrink, S. J.; Mark, A. E. *J. Phys. Chem. B* **2001**, 105, 6122–6127.

[50] Shinoda, W.; Okazaki, S. *J. Chem. Phys.* **109**, 109, 1517–1521.

[51] Almeida, P. F. F.; Vaz, W. L. C. In *Structure and Dynamics of Membranes: From Cells to Vesicles*; Lipowsky, R., Sackmann, E., Eds.; Elsevier: Amsterdam, 1995; pp 305–357.

[52] Vattulainen, I.; Mouritsen, O. G. In *Diffusion in Condensed Matter*; Kärger, J., Heitjans, P., Haberland, R., Eds.; Springer-Verlag: Berlin, 2003, In Press.

[53] Hansen, J.-P.; McDonald, I.R. *Theory of Simple Liquids. 2nd edition.* Academic Press: San Diego, 2000.

[54] Almeida, P. F. F.; Vaz, W. L. C.; Thompson, T. E. *Biochemistry* **1992**, 31, 6739–6747.

[55] Korlach, J.; Schwille, P.; Webb, W. W.; Feigenson, G. W. *Proc. Natl. Acad. Sci. USA* **1999**, 96, 8461–8466.

[56] Vaz, W. L. C.; Clegg, R. M.; Hallmann, D. *Biochemistry* **1985**, 24, 781–786.

[57] König, S.; Pfeiffer, W.; Bayerl, T.; Richter, D.; Sackmann, E. *J. Phys. II France* **1992**, 2, 1589–1615.

[58] Sackmann, E. In *Structure and Dynamics of Membranes: From Cells to Vesicles*; Lipowsky, R., Sackmann, E., Eds.; Elsevier: Amsterdam, 1995; pp 213–304.

[59] Tabony, J.; Perly, B. *Biochim. Biophys. Acta* **1990**, 1063, 67–72.

[60] Pastor, R. W.; Feller, S. E. In *Biological membranes: A molecular perspective from computation and experiment*; Merz, Jr. K. M., Roux, B., Eds.; Birkhäuser: Boston, 1996: pp 3–29.